Korean J Physiol Pharmacol 2025;29(1):67-81
https://doi.org/10.4196/kjpp.24.176

KJPP

Original Article

Mebendazole effectively overcomes imatinib resistance by dual-targeting BCR/ABL oncoprotein and β-tubulin in chronic myeloid leukemia cells

Li Yang[1], Zhuanyun Du[1], Yuhang Peng[1], Wenyao Zhang[1], Wenli Feng[1], and Ying Yuan[2,*]

[1]*Department of Clinical Hematology, Key Laboratory of Laboratory Medical Diagnostics Designated By the Ministry of Education, School of Laboratory Medicine, Chongqing Medical University,* [2]*Department of Respiratory and Critical Care Medicine, The First Affiliated Hospital of Chongqing Medical University, Chongqing 400016, China*

ARTICLE INFO

Received June 3, 2024
Revised July 4, 2024
Accepted July 10, 2024
Published online November 14, 2024

***Correspondence**
Ying Yuan
E-mail: yuanying@hospital.cqmu.edu.cn

Key Words
Chronic myeloid leukemia
Drug repositioning
Imatinib resistance
Mebendazole

ABSTRACT To target the pivotal BCR/ABL oncoprotein in chronic myeloid leukemia (CML) cells, tyrosine kinase inhibitors (TKIs) are utilized as landmark achievements in CML therapy. However, TKI resistance and intolerance remain principal obstacles in the treatment of CML patients. In recent years, drug repositioning provided alternative and promising perspectives apart from the classical cancer therapies, and promoted anthelmintic mebendazole (MBZ) as an effective anti-cancer drug in various cancers. Here, we investigated the role of MBZ in CML treatment including imatinib-resistant CML cells. Our results proved that MBZ inhibited the proliferation and induced apoptosis in CML cells. We found that MBZ effectively suppressed BCR/ABL kinase activity and MEK/ERK signaling pathway by reducing p-BCR/ABL and p-ERK levels with ABL1 targeting ability. Meanwhile, MBZ directly targeted the colchicine-binding site of β-tubulin protein, hampered microtubule polymerization and induced mitosis arrest and mitotic catastrophe. In addition, MBZ increased DNA damage levels and hampered the accumulation of ataxia-telangiectasia mutated and DNA-dependent protein kinase into the nucleus. This work discovered that anthelmintic MBZ exerts remarkable anticancer effects in both imatinib-sensitive and imatinib-resistant CML cells *in vitro* and revealed mechanisms underlying. From the perspective of drug repositioning and multi-target therapeutic strategy, this study provides a promising option for CML treatment, especially in TKI-resistant or intolerant individuals.

INTRODUCTION

Chronic myeloid leukemia (CML) is a clonal hematopoietic stem cell disorder with a characteristic Philadelphia chromosome and the presence of the bcr-abl fusion gene, which results from a reciprocal t(9;22) chromosomal translocation and encodes the principal pathogenetic protein BCR/ABL with constitutive tyrosine kinase activity [1,2]. The BCR-ABL oncoprotein hijacks downstream signaling pathways, including the JAK2/STAT, RAS/MEK/ERK, and PI3K/AKT pathways, which promote proliferation, inhibit differentiation, and maintain resistance to cell death [3]. Since being approved for CML treatment in 2001, tyrosine kinase inhibitors (TKIs) achieved remarkable treatment efficiency and significantly expanded the lifespan of CML patients [4]. However, approximately 40% of patients require a higher dose of imatinib (IM) or alternative agents after a period due to a lack

Author contributions: L.Y., W.F., and Y.Y. conceived and designed the experiments. L.Y. and Z.D. completed the experiments and wrote the manuscript. L.Y., W.F., and Y.Y. analyzed the data and results. Y.P. and W.Z. guided the experiment operation and were responsible for quality control. W.F. and Y.Y. reviewed the manuscript. W.F. and Y.Y. supervised the project and critically revised the manuscript. The final version of the manuscript was read and approved by all the authors. All authors agreed to the publication of this article.

of drug tolerance or resistance [5]. For years, there is always need for alternative therapy regimens for CML patients with TKI resistance or intolerance.

Drug repositioning is an attractive drug development strategy that aims to exploit the potentialities of existing drugs for alternative applications [6]. Belongs to benzimidazole broad-spectrum anthelmintics, mebendazole (MBZ) has been commonly prescribed for the treatment of intestinal helminthiasis since 1974 [7]. Increasing data in past decades has demonstrated that MBZ serves as an effective drug in preventing the aberrant tumorigenic characteristics of cancers including non-small lung cancer, colorectal cancer, breast cancer, head and neck cancer, neuroblastoma and leukemia *in vitro*, *in vivo* or *in silico* [8,9]. Recently, MBZ has entered clinical trials for the treatment of brain tumors and gastrointestinal cancer, and it is utilized to improve glioma cell sensitivity to traditional chemotherapy and radiotherapy while maintaining satisfactory tolerability [9-12]. Probable mechanisms and potential targets for MBZ have been investigated as research progressed. MBZ blocked microtubule organization and triggered G2/M arrest in various malignancies, similar to its action mechanisms in anti-parasite treatment. Moreover, MBZ could inhibit the Hedgehog pathway in the brain [13] and breast cancer [14], NOTCH1 signaling in T cell acute lymphoblastic leukemia cells [15], MEK/ERK pathway in hepatocellular carcinoma [16], melanoma [17] and acute myeloid leukemia [18]. These findings demonstrated that MBZ has a cell-type-specific function in anti-cancer efficacy, demanding additional investigation in specific cancers. Although MBZ has shown proliferative suppression in CML cells, the particular target has yet to be determined [18,19]. Interestingly, *in-silico* analysis [20] and kinase activity experiments [21-23] provide clues that MBZ can bind and inhibit ABL1 kinase activity, implying that MBZ can compromise BCR/ABL kinase activity.

In this study, we focused on the anti-cancer effect of MBZ on CML cells and investigated probable mechanisms. *In vitro* experiments were conducted using IM-sensitive K562 cells and IM-resistant K562/G01 cells as models. We tested the effects of MBZ on CML cells as well as the signaling pathways in CML cells. Based on our findings, we attempted to find out whether MBZ could potentially be employed as an alternative and supplementary medication in CML therapy, particularly in IM-resistant and intolerant individuals.

METHODS

Chemicals and antibodies

MBZ (Cat. No. M2523, ≥ 98% purity) was purchased from Sigma-Aldrich. Paclitaxel (Cat. No. T0968, ≥ 99% purity) and colchicine (Cat. No. T0320, ≥ 99% purity) were purchased from Targetmol. N, N′-ethylenebis(iodoacetamide) (EBI) (Cat. No. 7250-43-3, ≥ 99% purity) was purchased from Aladdin Industrial. MBZ, paclitaxel and colchicine were dissolved in 100% dimethyl sulfoxide (DMSO) at a concentration of 10 mM and stored at −80°C. The related antibodies were described below. Anti-Caspase3, anti-PARP, anti-c-abl, anti-phospho-c-abl, anti-STAT5, anti-phospho-STAT5, anti-p21, anti-c-Myc, anti-γH2AX, anti-ATM, anti-DNA-PKcs and anti-β-actin were purchased from Cell Signaling Technology. Anti-Bcl-2, anti-Bax, anti-Bcl-XL, anti-RAS, anti-phospho-RAF, anti-MEK, anti-phospho-MEK, anti-ERK, anti-phospho-ERK, anti-Cyclin B1, anti-α-tubulin, anti-β-tubulin, anti-GAPDH and anti-Lamin B1 were provided by Huabio.

Cell culture

Chronic myeloid cell line K562 and its IM-resistant derivative K562/G01 cell line (Cell Bank of Shanghai Institute of Cell Biology, Chinese Academy of Sciences) were maintained in RPMI-1640 medium (Gibco). Compared with the parental K562 cells, K562/G01 cells gained resistance through incubation with IM following the laboratory routine protocol [24]. Human bone marrow stromal cell line HS-5 (American Type Culture Collection) was cultured in Dulbecco's Modification of Eagle's Medium medium (Gibco). All cells were supplemented with 10% fetal bovine serum (Gibco) and 1% streptomycin/penicillin (Beyotime) and kept in a humidified 5% CO_2 chamber at 37°C.

Detection of proliferation by CCK-8 assay

Cell proliferation was analyzed using CCK-8 assay. K562, K562/G01, and HS-5 cells were seeded into a 96-well plate at a density of 4×10^3 cells/well and exposed to different concentrations of MBZ for 48 h. Following the incubation, 10 μl of CCK-8 solution was added to each well and the plates were incubated for 3 h. The optical density (OD) value at 450 nm was measured using a microplate reader (Bio-Tek). The MBZ concentrations resulting in a 50% inhibitory effect (IC_{50}) were determined based on these OD values. Results were expressed as a percentage of cell viability referred to the OD value measured in untreated cells, and the IC_{50} values were calculated with GraphPad Prism 8.0 software.

Colony formation assay

Cell self-renewal and proliferation ability were analyzed by colony formation assay. 100 cells were seeded into each well of 96 well plates and incubated with different concentrations of MBZ. After 7 days, colonies were counted, and the representative colony patterns were captured with a microscope.

Morphological alternations

Cell morphology was assessed using refined Wright's staining—Liu's staining. CML cells in each group were collected,

resuspended and plated onto glass slides. Then, the slides were left to dry at room temperature (RT) and stained with Liu's staining solution (Baso) according to the instructions. The slides were washed with tap water and air-dried before observation and photographed using a light microscope (Olympus) at a magnification of 400×. To quantitative analyze the degree of mitotic arrest, the mitotic index was represented as the ratio of mitosis cells to total cells, and at least 100 cells were counted in at least two random fields.

Western blot

After being treated with MBZ for 24 or 48 h, K562 and K562/G01 cells were lysed by RIPA buffer (Beyotime) with protease inhibitor PMSF (1%), phosphatase inhibitors NaF (1%) and Na_3VO_4 (1%), followed by centrifugation. Total protein concentrations were quantified using a Bicinchoninic Acid assay kit (Beyotime), and proteins were loaded on 8%–12% sodium dodecyl sulfate-polyacrylamide gel electrophoresis (SDS-PAGE) and transferred onto a PVDF membrane (Millipore). The membranes were blocked with 5% (w/v) fat-free milk and subsequently incubated with 1:1,000 dilution of specific primary antibodies at 4°C overnight and corresponding secondary antibodies at RT for 1.5 h. Detection was performed using an enhanced chemiluminescence system (Biosharp). The densities of bands were analyzed using ImageJ software (National Institutes of Health).

Cell cycle and apoptosis analysis

Cell Cycle Assay Kit and Annexin V-FITC/PI Apoptosis Kit (Elabscience) were used to detect the cell cycle distribution and the percent of apoptotic cells, respectively. K562 and K562/G01 cells (1×10^6) were planted into 6-well plates and treated with identified concentrations of MBZ for 24 h. To detect the cell cycle distribution, cells were collected and washed twice with phosphate-buffered saline (PBS), followed by fixed in 70% ethanol at 4°C overnight. Then genomic DNA was stained with propidium iodide (PI) reagent (50 μg/ml). The strength of red fluorescence was recorded in 488 nm using flow cytometer (CytoFLEX) and analyzed by CytExpert software v2.4.0.28 (Beckman Coulter Industry). For apoptosis analysis, cells were stained by Annexin V-FITC and PI staining (50 μg/ml) and subsequently measured by flow cytometer (CytoFLEX).

Immunofluorescence (IF) assay

Cells were fixed with 4% paraformaldehyde, permeabilized with 1% Triton X-100 for 15 min at RT, and blocked with goat serum at 4°C for 1 h. The cells were incubated with anti-α-tubulin or anti-γH2AX at 4°C overnight, followed by incubation with the Cy3 or FITC-labeled secondary antibody (Introvigen) and 4′,6-diamidino-2-phenylindole. Lastly, the slides were sealed with an anti-fading mounting medium (Solarbio). The representative photographs were acquired by a fluorescence confocal microscope (Nikon).

Tubulin polymerization assay

Polymerized (P) tubulin and soluble (S) tubulin were obtained as previously described [25]. After incubation, the cells were lysed in lysis buffer containing 20 mM Tris HCl (pH 6.8), 140 mM NaCl, 2 mM EDTA, 1 mM $MgCl_2$, 0.5% NP-40, and protease inhibitor PMSF and centrifuged at 13,000*g* for 10 min at RT to separate polymerized (P) tubulin from soluble (S) tubulin. Then the pellet containing polymerized (P) tubulin was re-suspended and lysed in RIPA buffer (Beyotime) and centrifuged at 13,000*g* for 15 min at 4°C, the supernatant containing depolymerized (S) tubulin was transferred to a new tube. Proteins were loaded, separated by 12% SDS-PAGE, and analyzed using western blotting with anti-α-tubulin antibody and anti-β-actin. The percentage of polymerized tubulin (%) was determined by dividing the band intensity values of polymerized tubulin by total tubulin.

Cellular thermal shift assay (CETSA)

CETSA was performed according to the experimental protocol [26]. In brief, after incubated with 10 μM MBZ or vehicle (DMSO) at 37°C for 1 h, K562, and K562/G01 cells were collected, rinsed, and resuspended in 1 ml PBS with protease inhibitor PMSF and heated with a range of temperature endpoints. The cells were subsequently lysed by three rounds of snap-freezing using liquid nitrogen and 25°C in a thermal cycle. After centrifuging at 13,000*g* for 20 min at 4°C, the supernatant was collected and used for western blotting. This experiment was performed at least three times, each on different days.

EBI competition assay

EBI competition assay was used to verify that MBZ interacts with the colchicine-binding site of β-tubulin. EBI can cross-link two cysteine residues at positions 239 and 354 of β-tubulin within the colchicine-binding site, thereby forming an EBI/β-tubulin adduct that can be distinguished from normal β-tubulin. EBI competition assay was performed according to the experimental protocol [27]. In brief, 6-well plates were seeded with either K562 and K562/G01 cells at 1×10^6 cells per well and incubated with MBZ and colchicine for 2 h, respectively. Then, EBI was added, and cells were treated with 100 μM EBI at the same conditions without changing the culture medium. After 1.5 h, cells were harvested to do a western blot analysis. GAPDH was utilized as the loading control of protein samples.

ABL1 kinase activity assay

The inhibitory activity of MBZ against the ABL1 kinase was determined by Caliper Mobility Shift Assays. Staurosporine was used as the reference drug. MBZ was prepared as 10 mM stock in 100% DMSO, followed by diluted in 100% DMSO to 100× final concentration. 5 μl of each DMSO was mixed with 95 μl 1× Kinase buffer (50 mM HEPES, 10 mM $MgCl_2$, 2 mM DTT and 0.01% Brij-35) for 10 min. In a 384-well plate, 5 μl of the diluted compound at varying concentrations (final concentrations 0.00000001-100 μM) were added in duplicate. 10 μl of enzyme solution (containing 2.25 nM ABL1) in 1× Kinase buffer was then added into each well and incubated at RT for 10 min. 10 μl of peptide solution containing FAM-labelled peptide (final concentration 3 μM FAM-P2) and ATP (final concentration 12 μM) in 1× Kinase buffer was added to each well to initiate the reaction, and then the mixture was incubated at 28°C. After one hour, the reaction was terminated by the addition of 25 μl stop buffer (100 mM HEPES, 50 mM EDTA, 0.2% Coating Reagent No. 3 [Caliper Life Science] and 0.015% Brij-35). These samples were then analyzed using Caliper EZ Reader II (Caliper Life Science) to collect conversion data.

Molecular docking

The initial crystal structures of tubulin complexed with colchicine (PDB: 4O2B) and BCR/ABL complexed with IM (PDB: 1IEP) were obtained from the RCSB Protein Data Bank [28]. MarvinSketch v23.11.0 software (Chemaxon) was used to build chemical structures for ligands, which were energetically minimized with UFF forcefield in Avogadro v1.2.0 software and prepared for docking in AutoDock tools. The possible binding sites and docked conformations were obtained when the ligand poses with the lowest docking energy using AutoDock Vina v1.1.2 software. Then, a protein-ligand interaction profiler was utilized to analyze the non-covalent interactions between the ligand and its target, which was visualized using PyMOL (http://pymol.org) [29]. Redocking reference ligands into their co-crystallized structure was performed before docking prediction. The root mean square deviation (RMSD) value between the crystallography conformation and predicted pose of the co-crystallized ligands were less than 1 angstrom (Å) without superimposing, which validates the reliability of the docking protocol and the accuracy of experimental results.

Nuclear extraction assay

Cytoplasmic protein and nuclear protein extraction were obtained using the Nuclear Protein Extraction Kit (Beyotime) according to the manufacturer's instructions. The cytoplasmic and nuclear components were then subjected to western blot. Expression of β-tubulin and Lamin B1, as loading control for cytoplasm and nucleus, was assessed using their specific monoclonal antibodies.

Statistical analysis

Statistical analysis was performed by GraphPad Prism 8.0. All data were presented as the mean and standard deviation of at least three independent experiments with essentially the same results. Student's t-test was conducted to assess the statistical difference between two groups and one-way ANOVA was used among multiple groups. p-values < 0.05 were considered statistically significant.

RESULTS

MBZ inhibits proliferation and induces apoptosis of CML cells

We used the CCK-8 assay to compare the antiproliferative effects of MBZ and IM on the IM-resistant CML cell line K562/G01 and its parental K562. When both cells were treated with IM, there was dose-dependent inhibition of cell viability (Fig. 1A, B), but the IC_{50} for K562/G01 cells was ten times higher than IM-sensitive parental K562 cells. Close to the IC_{50} of IM (0.35 μM), MBZ exhibited a cytotoxic effect against K562 cells with an IC_{50} at 0.38 μM. Meanwhile, MBZ presented an IC_{50} at 0.84 μM against IM-resistant K562/G01 cells, which is six times lower than the IC_{50} of IM in the same cell group (5.44 μM) (Fig. 1C). Using the normal bone marrow mesenchymal stem cell line HS-5 as a control, even when its concentration reached 10 μM for 48 h, MBZ showed limited cellular toxicity (Fig. 1D). Similarly, MBZ showed an obvious inhibitory effect on the number and size of colonies formed by K562 and K562/G01 cells (Fig. 1E, F), which was consistent with the data in Fig. 1C.

To evaluate drug-induced apoptosis in CML cells, we conducted annexin-V-FITC/PI labeling and flow cytometry assays. As shown in Fig. 1G, H, after the co-incubation of K562 and K562/G01 with MBZ at 0.5 μM or 1.0 μM for 24 h, apoptosis was detected. At the same concentrations, the cleavages of Caspase-3 and its substrate PARP were also detected with immunoblotting (Fig. 1I). Moreover, because of upregulated pro-apoptotic protein Bax and downregulated anti-apoptotic Bcl-2 and Bcl-XL (Fig. 1J), Bcl-2/Bax ratio were reduced in both cells (Fig. 1K).

MBZ suppresses BCR/ABL kinase activity and downstream signaling pathways by binding the ATP-binding site of BCR/ABL kinase

MBZ was demonstrated to inhibit ABL1 kinase activity [21-23] and target the ATP-binding site in BCR/ABL in previous studies [20]. As depicted in Fig. 2A, CML cells treated with 0.5 μM and 1.0

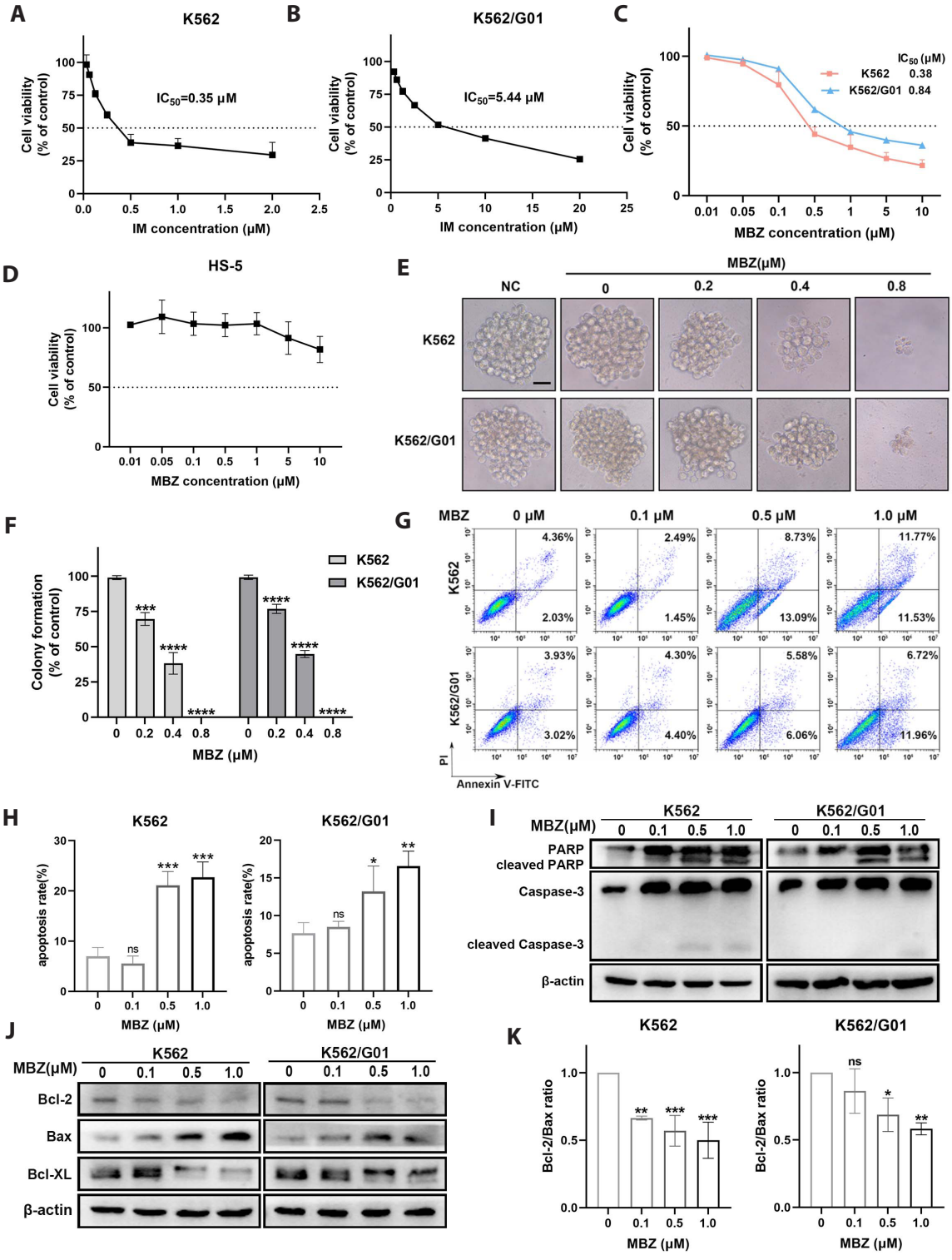

Fig. 1. Mebendazole (MBZ) inhibits proliferation and induces apoptosis of CML cells. (A–C) Dose-response curve for IM and MBZ in K562 and K562/G01 using CCK-8 assay after incubation for 48 h. (D) Dose-response curve for MBZ in bone marrow stromal cell line HS-5 using CCK-8 assay after incubation for 48 h. (E) The cell proliferative activity of CML cells treated with MBZ for 7 days was assessed using a colony formation assay. The scale bar represents 25 μm. (F) The colony formation rate was calculated and statistically analyzed. (G) The apoptosis levels of CML cells were evaluated using annexin-V-FITC/PI labeling and FCM after MBZ treatment for 24 h. (H) The cell apoptosis rate was analyzed based on the FCM results. (I) The protein expression levels of PARP, Caspase-3, and their corresponding cleaved bands were measured using a western blot. (J, K) The expression levels of Bax, Bcl-2, and Bcl-XL were detected by western blot, and the ratio of Bcl-2/Bax was calculated. The values are the mean and SD of three independent experiments. CML, chronic myeloid leukemia; IM, imatinib; PI, propidium iodide; FCM, flow cytometry; ns, no significance. *p < 0.05, **p < 0.01, ***p < 0.001 and ****p < 0.0001 *vs*. the control group.

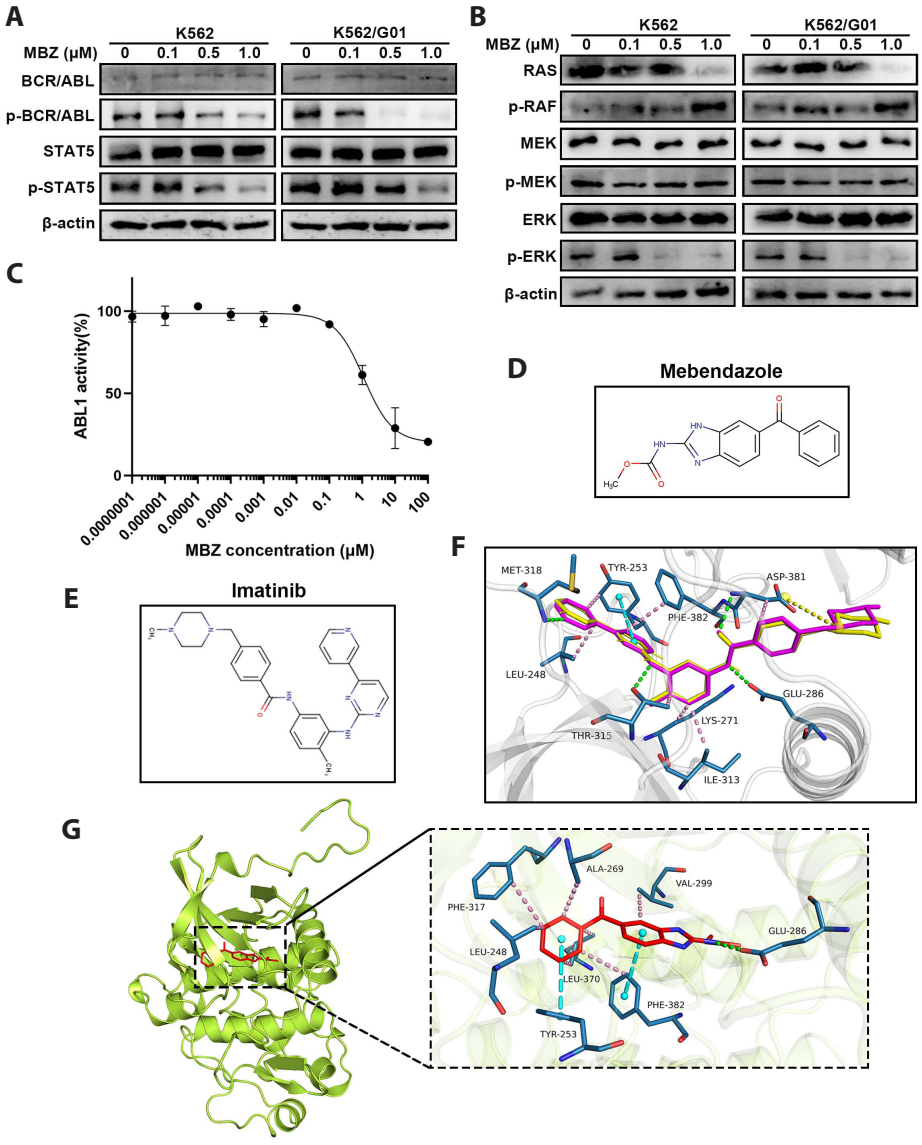

Fig. 2. Mebendazole (MBZ) suppresses BCR/ABL kinase activity and downstream signaling pathways by binding the ATP-binding site of BCR/ABL kinase. (A, B) Western blot was used to measure protein expression of BCR/ABL, p-BCR/ABL, STAT5, p-STAT5 and signaling molecules in the RAS/RAF/MEK/ERK signaling pathway after MBZ treatment for 24 h. (C) *In vitro* validation of protein kinase inhibition by MBZ. Staurosporine was used as a positive control to inhibit the kinase activity of ABL1. The values are the mean ± SD of three independent experiments. (D) The molecular structure of MBZ. (E) The molecular structure of imatinib. (F) The binding pose and interactions of imatinib (magenta) with co-crystallized BCR/ABL kinase in the crystal structure (PDB ID: 1IEP) and predicted docking orientation of imatinib (yellow) *in silico* docking analysis. (G) The predicted binding pose of MBZ (red) in BCR/ABL tyrosine kinase (green, PDB ID: 1IEP) with a binding affinity of –9.0 kcal/mol. Key amino acid residues are visualized in sticks. Hydrogen bonds (green), hydrophobic interactions (pink), π-stacking (cyan) and salt bridges (yellow) are indicated as dashed lines.

μM MBZ downregulated p-BCR/ABL and p-STAT5 with stably expressed BCR/ABL and STAT5. Moreover, treatment with MBZ significantly decreased the expression of RAS and p-ERK1/2 in both cells (Fig. 2B).

To investigate the association between MBZ and BCR/ABL, we first assessed MBZ's kinase inhibition ability against BCR/ABL using ABL1 kinase activity assay. In Fig. 2C, MBZ strongly suppressed ABL1 kinase activity with an IC_{50} of 1.78 μM, indicating MBZ could regulate ABL1 kinase activity. Then, a molecular docking assay was performed to estimate the possible binding mode between MBZ (Fig. 2D) and BCR/ABL (PDB code: 1IEP). The RMSD value of the highest-ranked orientation of IM (Fig. 2E) from its crystallography conformation was found to be 0.87 Å (Fig. 2F), validating the available docking protocol in this study [30]. The docking results showed that MBZ fitted within the ATP-binding site of BCR/ABL (–9.0 kcal/mol) and underwent hydrogen bonding with GLU-286 and van der Waals interactions with the surrounding amino acid residues LEU-248, ALA-269, VAL-299, PHE-317, LEU-370 and PHE-382 (Fig. 2G). In addition, aromatic rings of MBZ were predicted to make π-stacking

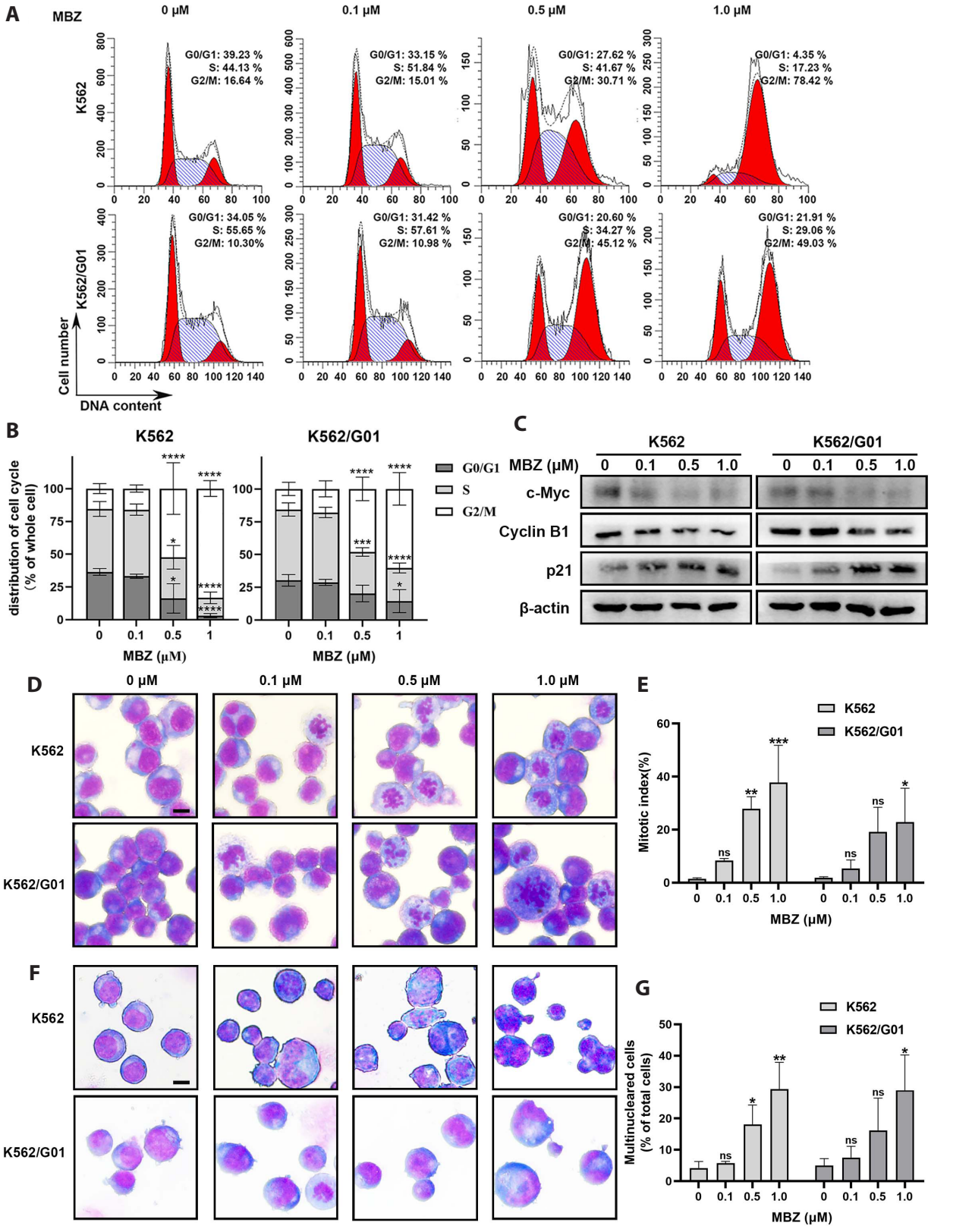

Fig. 3. Mebendazole (MBZ) induces aberrant mitosis and multinucleation in CML cells. (A, B) Cell cycle distribution was measured and analyzed using FCM. (C) The expression levels of cell cycle-associated proteins c-MYC, p21 and Cyclin B1 in CML cells treated with MBZ for 24 h were detected by western blot. (D, F) Morphological changes were observed by Liu's staining after incubation with MBZ for 24 h (D) and 36 h (F). The scale bar represents 10 μm. (E, G) Mitotic index was determined by the proportion of mitotic cells after treatment with MBZ for 24 h and multi-nucleated cells were counted after 48 h (in a total of at least 100 cells in at least two random fields). The values are represented as the mean ± SD of three independent experiments. CML, chronic myeloid leukemia; FCM, flow cytometry; ns, no significance. *p < 0.05, **p < 0.01, ***p < 0.001 and ****p < 0.0001 *vs*. the controls.

interaction with the aromatic ring from TYR-253 and PHE-382, respectively.

MBZ induces aberrant mitosis and multinucleation in CML cells

Flow cytometry was performed to explore how MBZ affects cell cycle progression. We found that MBZ increased the CML cells in the G2/M phase (Fig. 3A, B). The results were consistent with the upregulation of the cell-cycle inhibitor p21 and the downregulation of cyclin B1 and c-MYC (Fig. 3C).

To determine which phase CML cells were mainly blocked in, we explored the morphological changes following MBZ incubation. Some MBZ-treated CML cells exhibited a prophase-like morphology, with agglutinated chromosomes and vanished nuclear envelope (Fig. 3D), which implied chromosome congression and segregation errors were triggered. As shown in Fig. 3E, 2% of cells were in mitosis in the untreated control, which increased to 30% in K562 cells and 20% in K562/G01 cells following 24 h of exposure to 0.5 or 1.0 μM MBZ (Fig. 3E).

According to previous research, mitotic catastrophe is frequently accompanied by mitosis arrest and generates unique nuclear modifications that result in multinucleation and/or micronucleation, which are regarded as critical morphological signs for detection [31]. Microscope inspection after 36 h of treatment revealed that diploid and polyploid cells were significantly accumulated in K562 cells following incubation with 0.5 μM MBZ, and to a greater extent with 1.0 μM (Fig. 3F). In K562/G01 cells, there was a lesser but still significant accumulation of multinucleated cells (Fig. 3G).

MBZ disrupts microtubule organization and leads to tubulin polymerization

Since mitosis is a cell-cycle event that is extremely dependent on the normal functional microtubule, we used IF and confocal microscopy to examine the effects of MBZ on α-tubulin protein distribution and microtubule network. We found, in untreated controls, a well-assembled network containing microtubule protein typically spread in the cytoplasm (Fig. 4A, E). However, after 24 h of treatment with 0.5 μM (Fig. 4C, G) or 1.0 μM (Fig. 4D, H) MBZ, the microtubule network displayed significant abnormal arrangement and α-tubulin was unevenly distributed in CML cells.

Furthermore, a fragmented nuclear area appeared in exposed cells, similar to the cytomorphology alternations shown in Liu's staining (Fig. 3D), and was surrounded by aggregated α-tubulin protein and aberrant multipolar α-tubulin structures with disrupted microtubular organization (Fig. 4C, D and Fig. 4G, H), but no difference in α-tubulin total protein levels was observed (Fig. 4I). The inhibitory effect of MBZ on tubulin assembly dynamics was then investigated further by measuring the levels of polymerized and depolymerized α-tubulin. As positive controls, paclitaxel increased α-tubulin polymerization while colchicine decreased it. Results showed that MBZ treatment decreased the level of polymerized α-tubulin at 0.5 and 1.0 μM in CML cells (Fig. 4J-M).

MBZ effectively interacts with the colchicine-binding site of β-tubulin

We guessed that MBZ could depolymerize tubulin by binding with it, which was preliminarily confirmed by the CETSA. After preincubated for 1 h with 10 μM MBZ, the thermostability of the β-tubulin protein was increased, and noticeable shifts in the melting curves were observed (Fig. 5A, B). Then, a molecular docking assay was performed to estimate the possible docking orientation between MBZ (Fig. 2D) and tubulin (PDB code: 4O2B). The RMSD value between the highest-ranked orientation and the initial position of colchicine (Fig. 5C) was found to be 0.090 Å (Fig. 5D), suggesting this docking protocol was valid. The docking results exhibited that MBZ displayed a perfect fitting pose within the colchicine-binding site of α/β-tubulin heterodimer (–10.1 kcal/mol) and undergoes hydrogen-bonding and van der Waals interactions with the surrounding amino acid residues (Fig. 5E). More precisely, the carbamate–benzimidazole moiety was expected to make five hydrogen bonds with ASN-101, SER-140, GLY-143, GLU-183 and LEU-24`8, and both aromatic rings of MBZ was also predicted to form five hydrophobic interactions with LEU-248, LYS-254, ASN-258 and LYS-352.

Furthermore, the EBI competition assay was performed in a cellular context to assess the binding of MBZ to the colchicine-binding site. Incubation with a colchicine-binding site inhibitor prior to EBI could prevent the formation of the EBI/β-tubulin adduct [27]. As the results showed, the formation of EBI: β-tubulin adducts was prevented in CML cells after preincubation with 10 or 20 μM MBZ before EBI incubation (Fig. 5F), suggesting MBZ effectively interacts with β-tubulin at the colchicine-binding site in CML cells.

MBZ enhances DNA damage by hindering the recruitment of ataxia-telangiectasia mutated (ATM) and DNA-dependent protein kinase (DNA-PKcs) in the nucleus

Mitotic catastrophes can be effectively triggered by not only delayed mitosis but also DNA damage [32]. To check whether MBZ can cause DNA damage in CML cells, we employed immunoblotting and IF and observed dramatically elevated protein expression and nucleus location of γH2AX, an established marker of DNA damage, after 24 h treatment with 0.5 and 1.0 μM MBZ (Fig. 6A, B). Given the crucial role of inducible endogenous reactive oxygen species (ROS) in DNA damage, we measured ROS levels in MBZ-treated CML cells using DCFH-DA fluorescent probe labeling and flow cytometry detection, but there was no signifi-

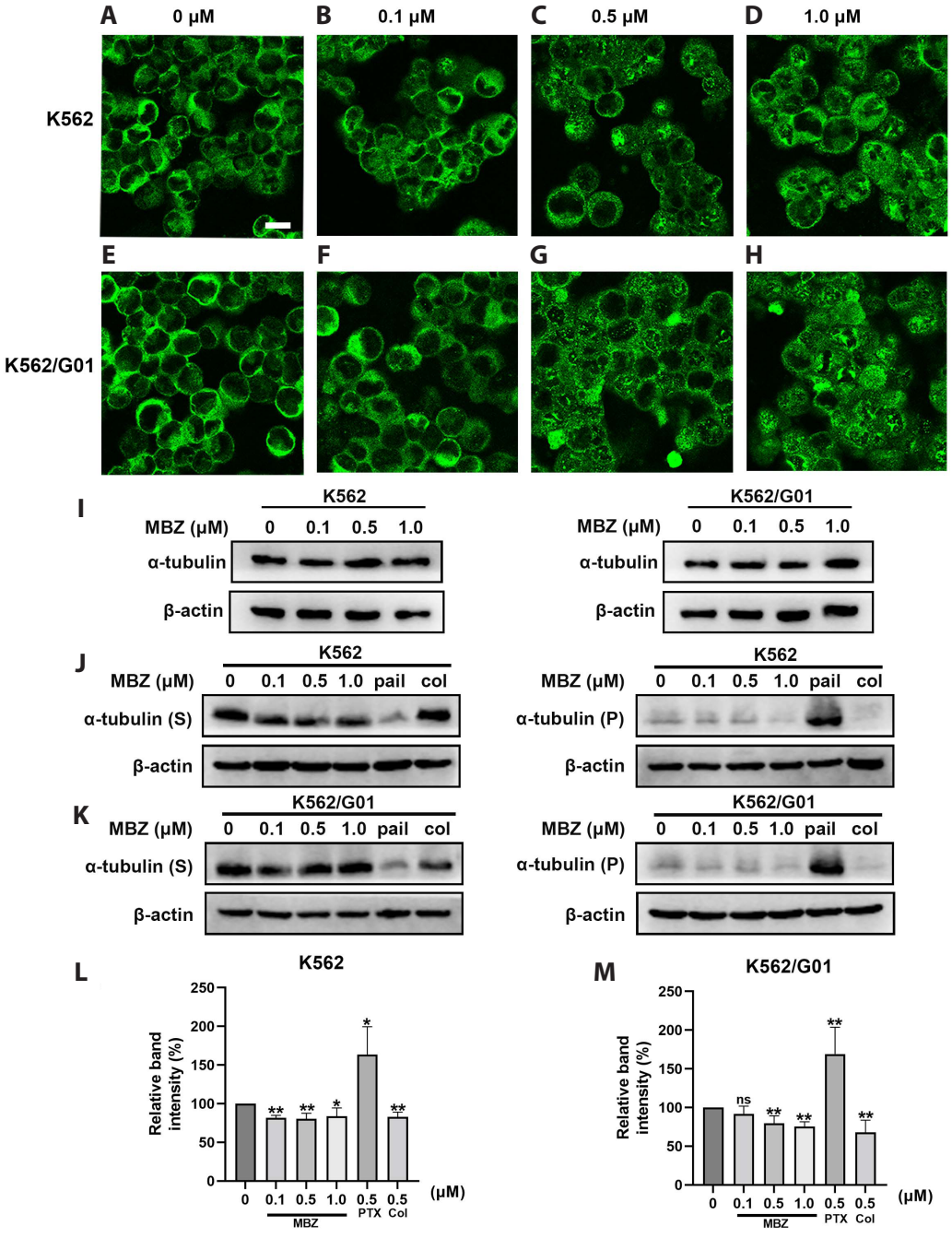

Fig. 4. Mebendazole (MBZ) disrupts microtubule organization and leads to tubulin polymerization. (A, E) DMSO; (B, F) 0.1 μM MBZ; (C, G) 0.5 μM MBZ; (D, H) 1.0 μM MBZ. CML cells were treated with the indicated concentrations of MBZ for 24 h, and the alternation of microtubule organization and distribution was observed by fluorescence confocal microscopy. The scale bar represents 10 μm. (I) The protein level of α-tubulin in CML cells was detected by western blot. Tubulin polymerization assay was utilized to evaluate the polymerized (P) and soluble (S) α-tubulin in K562 cells (J) and K562/G01 cells (K) after incubated with MBZ, colchicine (Col), or paclitaxel (PTX) at indicated concentrations. The percentage of polymerized α-tubulin in K562 cells (L) and K562/G01 cells (M) was determined using the formula: %P = P/(P + S). The values are the mean ± SD of four independent experiments. CML, chronic myeloid leukemia; DMSO, dimethyl sulfoxide; ns, no significance. *p < 0.05 and **p < 0.01 *vs*. the controls.

cant increase in both cells (Fig. 6C). Meanwhile, we evaluated the expression of the DNA repair proteins ATM and DNA-PKcs, which are important DNA damage repair players in homologous recombination and non-homologous end-joining, respectively, but there was no significant decrease in both of proteins (Fig. 6D). We questioned if ATM and DNA-PKcs constantly recruited into the nucleus following MBZ-induced DNA damage for 24 h. Then, nuclear and cytoplasmic protein extraction assays and western blot assay results showed that MBZ treatment resulted in enhanced cytoplasm distribution of ATM and DNA-PKcs at 0.5

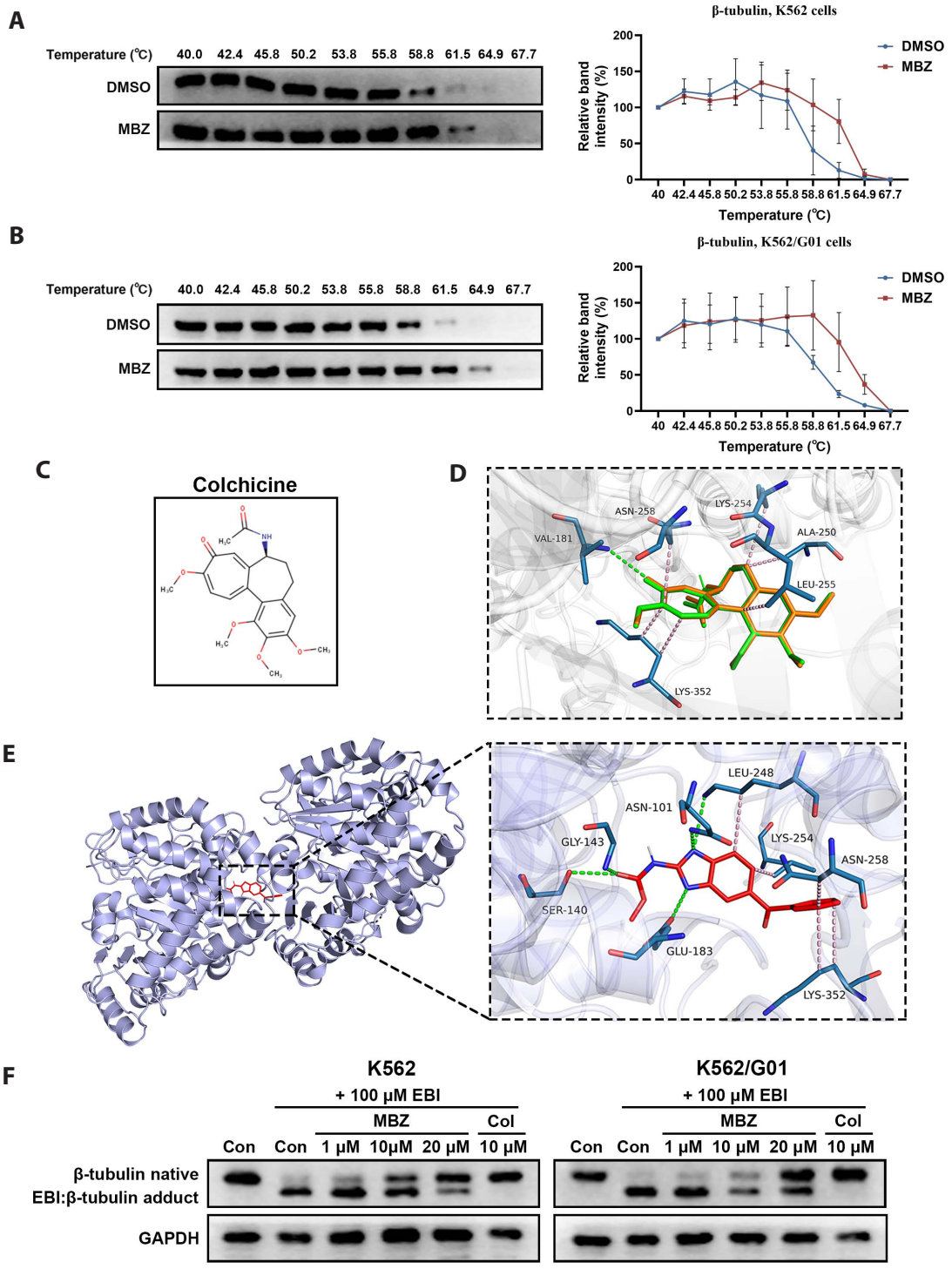

Fig. 5. Mebendazole (MBZ) effectively interacts with the colchicine-binding site of β-tubulin. (A, B) β-tubulin protein levels in CML cells were detected using CETSA and the quantitative data were shown on the right. The values are the mean ± SD of three independent experiments. (C) Molecular structures of colchicine. (D) The binding pose of colchicine (orange) with tubulin in the crystal structure (PDB ID: 4O2B) and predicted orientation of colchicine (green) *in silico* docking analysis. (E) The predicted binding orientation and interactions of MBZ (red) in the α/β-tubulin heterodimer (purple, PDB ID: 4O2B) with a binding affinity of −10.1 kcal/mol. Key amino acid residues are visualized in sticks. Hydrogen bonds (green), and hydrophobic interactions (pink) are indicated as dashed lines. (F) The levels of active β-tubulin and EBI: β-tubulin adduct were detected by CETSA and western blot. CML, chronic myeloid leukemia; CETSA, cellular thermal shift assay; EBI, N, N′-ethylenebis(iodoacetamide); DMSO, dimethyl sulfoxide.

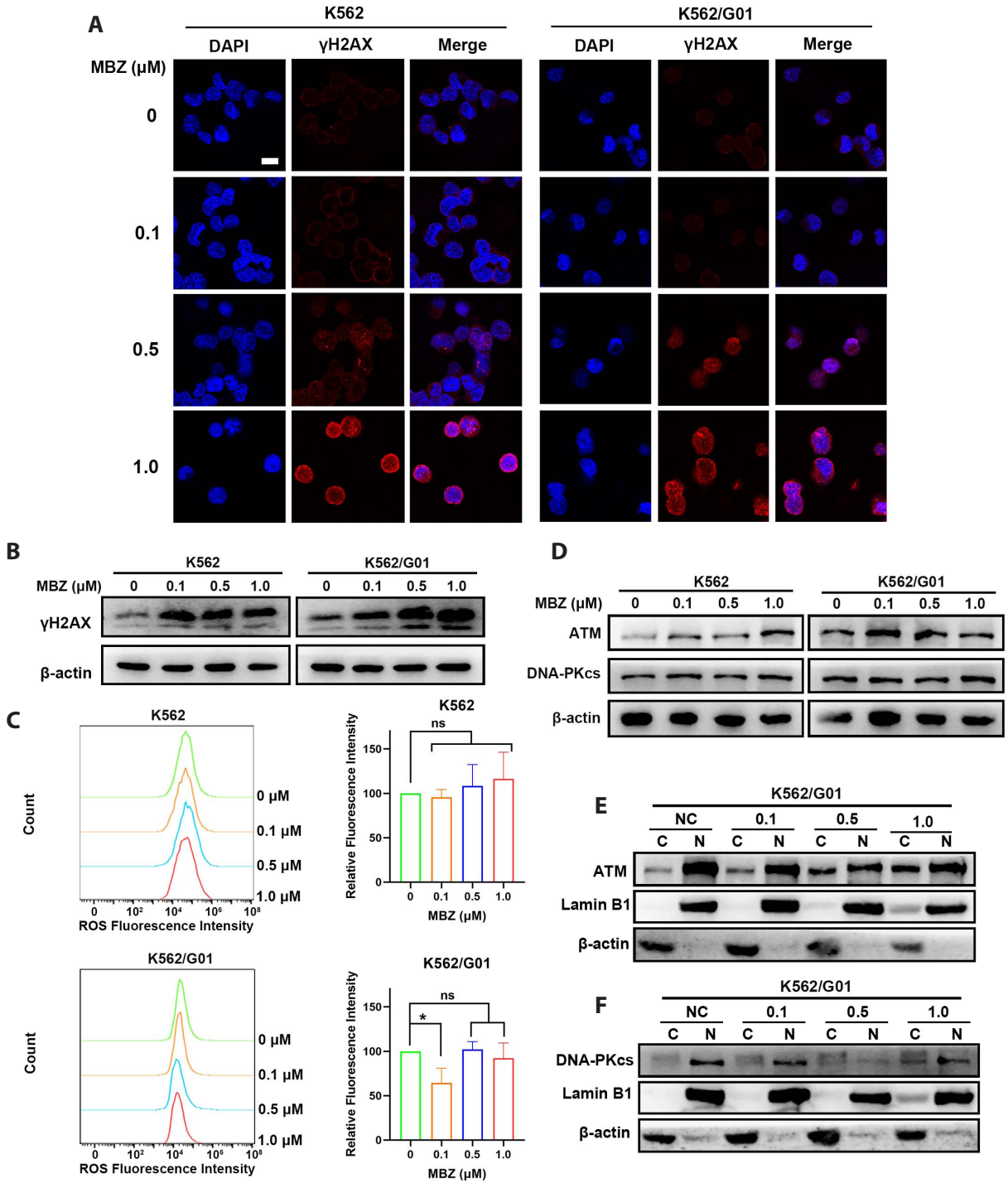

Fig. 6. Mebendazole (MBZ) enhanced DNA damage by hindering the recruitment of ATM and DNA-PKcs in the nucleus. (A, B) The alternation of the cellular location and protein levels of γH2AX in CML cells after treatment with MBZ for 24 h was screened by immunofluorescence and western blot. The scale bar represents 10 μm. (C) The levels of ROS were evaluated by FCM. *$p < 0.05$ *vs*. the control group. (D) The expression levels of DNA repair protein ATM and DNA-PKcs were assessed by western blot. (E, F) Nuclear and cytoplasmic protein extraction assay was performed and followed by western blot to analyze the cellular accumulation of ATM (E) and DNA-PKcs (F) in the cytoplasm (C) and nucleus (N) in K562/G01 cells. ATM, ataxia-telangiectasia mutated; DNA-PKcs, DNA-dependent protein kinase; CML, chronic myeloid leukemia; ROS, reactive oxygen species; FCM, flow cytometry; ns, no significance.

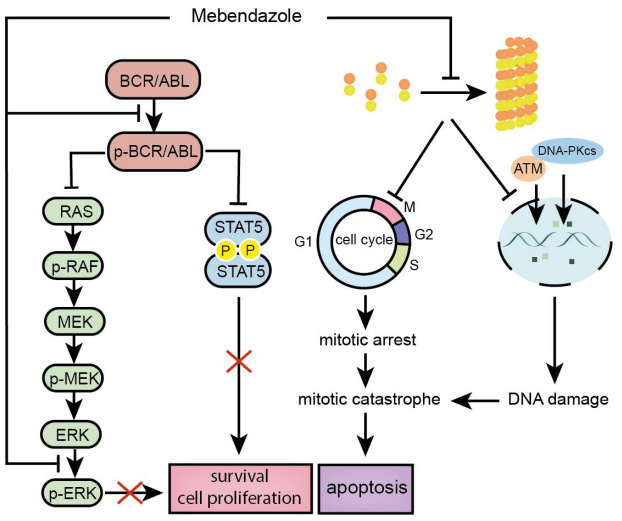

Fig. 7. Schematic diagram of the function and mechanisms of MBZ in CML cells. The anticancer effect of MBZ is mediated by at least two processes: one involving downregulated p-BCR/ABL and its downstream signaling pathways, and the other involving disrupted microtubule dynamics. This molecule downregulates p-BCR/ABL, p-STAT5 and MAPK signalling pathway, thereby inhibiting the growth of CML cells. MBZ blocks microtubule polymerization, results in cell cycle arrest at mitosis and triggers mitotic catastrophe event, which induces apoptosis in CML cells. In addition, MBZ triggers substantial DNA damage by delaying repair processing, leading to enhanced genomic instability and mitotic catastrophe. MBZ, mebendazole; CML, chronic myeloid leukemia; ATM, ataxia-telangiectasia mutated; DNA-PKcs, DNA-dependent protein kinase.

and 1.0 μM (Fig. 6E, F).

DISCUSSION

CML is a myeloproliferative disease defined by the formation of BCR/ABL oncoprotein, which is the primary target of IM, an established TKI. Although IM has been widely used for CML treatment and has significantly enhanced life expectancy, there is an increased rate of recurrence and resistance, prompting the development of second and third-generation TKIs. TKI resistance and intolerance, on the other hand, remain major obstacles to CML treatment. As a result, finding an alternative therapy for TKI-resistant or intolerant CML patients is crucial. In this study, we discovered that anthelmintic MBZ exhibited a notable inhibitory effect on both IM-sensitive and IM-resistant CML cells. From the perspective of drug repurposing, this study provides a promising option for CML treatment in TKI-resistant or intolerant individuals.

The anthelmintic MBZ was formerly thought to be a promising repurposing medicine due to its potent anticancer effect in various cancers, despite the fact that anticancer mechanisms differ between cancer types. Here we demonstrated that MBZ exerts a remarkable anticancer effect in IM-sensitive and IM-resistant CML cells through several synergistic mechanisms (Fig. 7). MBZ inhibits CML cell proliferation by suppressing BCR/ABL kinase activity and its downstream MAPK signaling pathways by targeting the ATP-binding site of BCR/ABL. Furthermore, MBZ binds to the colchicine-binding site of β-tubulin, causing aberrant microtubule function, arresting CML cells in the mitotic phase, and triggering a mitotic catastrophe event.

As the characterized oncoprotein of CML, BCR-ABL is always a major target for treatment and has an activation effect on downstream signaling pathways, including STAT5, RAS/MEK/ERK, and PI3K/AKT, to enhance malignancy features [3]. Previous researches have shown that MBZ can inhibit ABL1 kinase activity and directly bind to the ATP-binding site of the BCR/ABL protein [20-23], which is consistent with our data. Nevertheless, MBZ's inhibition effect on BCR/ABL kinase activity and its downstream signaling pathways remains unidentified. Our findings showed that MBZ greatly decreases the phosphorylation levels of BCR/ABL and STAT5. Although the major resistance mechanism of K562/G01 pertains to BCR/ABL overexpression, we failed to observe a substantially different inhibitory impact in the same concentration when compared to K562. The result suggested that MBZ could exert a potent inhibitory effect on the phosphorylation level of BCR-ABL at least at the dose of 0.5 μM. Furthermore, MBZ reduced RAS protein expression and increased p-RAF level. Previous studies have indicated that MBZ could downregulate protein levels by affecting several different molecular biology processes. Chen *et al*. [33] showed that MBZ reduced deubiquitinase USP5 expression, leading to increased levels of oncogenic transcription factor c-Maf ubiquitination and subsequent degradation of the c-Maf. Moreover, Freisleben *et al*. [34] demonstrated that MBZ could attenuate GLI transcription factors promoter activity and promote the proteasomal degradation of GLI *via* inhibition of HSP70/90 chaperone activity. Considering these challenges in directly targeting RAS and the complex regulatory mechanisms of its post-translational modifications [35,36], we hypothesize that the altered RAS protein level may be an indirect result of regulatory impact of MBZ, including reduced promoter activity, abnormal protein modification, and disturbed proteasomal degradation pathways. This hypothesis needs to be further verifed by subsequent experiments. Previously, Hentschel *et al*. [37] showed that RAF was BCR/ABL- and RAS-independent activated in IM-resistant CML cells. Similarly, Ma *et al*. [38] revealed IM-resistant K562 cells had sustained p-RAF expression and MEK/ERK pathway after IM treatment. Therefore, it is possible that increased p-RAF expression is a response to inhibited BCR/ABL kinase activity and help cells escape from apoptosis by sustaining downstream MEK/ERK pathway after MBZ treatment. However, although p-RAF expression appeared to be restored by some RAS-independent mechanism, and the protein levels of MEK and ERK remained intact, ERK1/2 phosphorylation was stably and efficiently inhibited. A study by Younis *et al*. [16] found that MBZ blocked the RAS/RAF/MEK/ERK pathway at the last

step (ERK1/2 phosphorylation) in hepatocellular cancer. As a result, we hypothesized that MBZ might reduce the amount of p-ERK1/2 by the indirect effect of defective BCR/ABL oncoprotein and direct suppression of MBZ, which needs to be confirmed in future investigations.

Our findings showed that MBZ generated aberrant α-tubulin distribution and defective α-tubulin structures in both CML cells. However, no difference in α-tubulin protein levels was identified. Therefore, we predicted that MBZ could influence tubulin state alternation between polymerization and depolymerization. We found that MBZ depolymerized α-tubulin, implying that MBZ altered microtubule dynamic instability and impeded α-tubulin polymerization in the cellular environment. Recent studies suggest that MBZ can hinder tubulin polymerization and induce mitotic arrest in brain tumors, ovarian cancer, and triple-negative breast cancer [25,39,40], which is consistent with our findings. The CETSA revealed that preincubating β-tubulin with MBZ improved its thermal stability, revealing a possible interaction between MBZ and β-tubulin. Hence, we speculated that MBZ interrupted tubulin polymerization by directly binding tubulin. The molecular docking analysis of MBZ and tubulin heterodimer suggested that MBZ might dock into the β-tubulin colchicine-binding site. To verify the docking result, an EBI-competition assay was carried out and the results exhibited that preincubation with MBZ could inhibit the formation of EBI: β-tubulin adduct. These data demonstrate that MBZ acts as an effective tubulin polymerization inhibitor by targeting the colchicine-binding site of β-tubulin.

Docking models of MBZ bound to BCR/ABL and tubulin were also studied to understand the structural properties of the dual-targeting agent. In previous studies, it was found that methyl benzimidazole carbamates inhibitors fungicides, such as carbendazim, could bind to the β-tubulin of pathogenic bacteria [41]. Here, binding mode analyses also revealed that benzimidazole carbamates moiety of MBZ engaged in the formation of hydrogen bonds with the surrounding residues, which seems to make the most significant contribution toward stabilizing MBZ in the colchicine-binding sites, implying the potential interaction between benzimidazole carbamates moiety and tubulin. Besides, in order to help stabilize the binding of MBZ, both aromatic rings of MBZ were predicted to make hydrophobic interactions with nonpolar residues in both binding mode, and formed π-stacking interactions in the ATP-binding sites of BCR/ABL. These computational findings may provide insight into the design of new potent dual-target inhibitors as anti-cancer drugs through de novo design and Structure-Activity Relationships studies based on the MBZ scaffold.

MBZ has previously been used in combination with DNA-damaging agents or ionizing radiation to improve the efficacy of chemotherapy or radiotherapy in newly diagnosed high-grade or temozolomide-resistant glioma [42], malignant meningioma [43], and IR-resistant triple-negative breast cancer [44]. It suggested that MBZ could be able to sensitize tumor cells to DNA damage-inducing agents. In this work, we discovered that MBZ significantly enhanced the quantity of γH2AX and promoted its nuclei recruitment, suggesting the accumulation of DNA damage. Considering the crucial role of inducible endogenous ROS in DNA damage and DNA damage repair protein ATM and DNA-PKcs, we evaluated the ROS levels and the total protein levels of ATM and DNA-PKcs, but no significant increase was observed in both cell lines. The protein levels of key DNA damage repair molecules can be maintained in the nucleus to ensure normal and efficient DNA repair processing. Hence, we explored the distribution of DNA repair molecules in CML cells and found MBZ could impede the rapid recruitment of ATM and DNA-PKcs after significant DNA damage accumulation. Markowitz and his colleagues [44] studied that MBZ could radiosensitize glioma cells by disturbing the trafficking of DNA damage repair proteins NBS1 and CHK2. Their study verified that MBZ disrupted the trafficking of DNA damage repair molecules in an interphase cell after radiosensitization. In this study, we demonstrated that dramatically enhanced genome instability could be observed in CML cells under the monotherapy of MBZ. However, whether MBZ can prevent ATM and DNA-PKcs from recruiting into DNA repair sites in the next interphase requires additional investigation.

Drug repurposing has recently come under the spotlight to maximize the benefits of current medical resources, minimize expenses, and shorten the research period. This study extensively investigated the association between MBZ and CML *in vitro*, manifested the potential of substitute therapeutic strategies in IM-resistant CML cells, as well as the efficiency of MBZ as an anti-cancer agent, and notably, revealed various molecular targets and anti-cancer mechanisms. According to the drug repurposing concept, our findings establish a foundation for the future application of MBZ for CML patients, particularly for overcoming IM resistance or serving as the late-line treatment following TKI resistance. By embracing different anti-tumor mechanisms of MBZ, we widen rather than constrain our horizons on multi-target therapy.

In conclusion, our studies revealed that MBZ inhibited the BCR/ABL and its downstream MAPK signaling pathways with BCR/ABL kinase suppressive activities in IM-sensitive and IM-resistant CML cells. MBZ bound to the colchicine-binding site of β-tubulin, blocking microtubule polymerization, resulting in cell cycle arrest at mitosis, and leading to mitotic catastrophe. In addition, MBZ triggered substantial DNA damage in CML cells, leading to enhanced genomic instability during aberrant mitotic progression. This study lays a foundation for clinical validation of MBZ as a possible drug for CML patients confronted with IM resistance or intolerance.

FUNDING

This work is supported by the Chongqing Young and middle-aged Medical Talents Programme (2022GDRC012), the Youth Top Science and Technology Talent Fund Project of The First Affiliated Hospital of Chongqing Medical University (BJRC2020–04), and the Innovation Support Program for Overseas Students of Chongqing (cx2018142).

ACKNOWLEDGEMENTS

None.

CONFLICTS OF INTEREST

The authors declare no conflicts of interest.

REFERENCES

1. Mughal TI, Radich JP, Deininger MW, Apperley JF, Hughes TP, Harrison CJ, Gambacorti-Passerini C, Saglio G, Cortes J, Daley GQ. Chronic myeloid leukemia: reminiscences and dreams. *Haematologica*. 2016;101:541-558.
2. Chereda B, Melo JV. Natural course and biology of CML. *Ann Hematol*. 2015;94 Suppl 2:S107-121.
3. Kang ZJ, Liu YF, Xu LZ, Long ZJ, Huang D, Yang Y, Liu B, Feng JX, Pan YJ, Yan JS, Liu Q. The Philadelphia chromosome in leukemogenesis. *Chin J Cancer*. 2016;35:48.
4. Bower H, Björkholm M, Dickman PW, Höglund M, Lambert PC, Andersson TM. Life expectancy of patients with chronic myeloid leukemia approaches the life expectancy of the general population. *J Clin Oncol*. 2016;34:2851-2857.
5. Innes AJ, Milojkovic D, Apperley JF. Allogeneic transplantation for CML in the TKI era: striking the right balance. *Nat Rev Clin Oncol*. 2016;13:79-91.
6. Sultana T, Jan U, Lee JI. Double repositioning: veterinary antiparasitic to human anticancer. *Int J Mol Sci*. 2022;23:4315.
7. Nath J, Paul R, Ghosh SK, Paul J, Singha B, Debnath N. Drug repurposing and relabeling for cancer therapy: Emerging benzimidazole antihelminthics with potent anticancer effects. *Life Sci*. 2020;258:118189.
8. Čáňová K, Rozkydalová L, Rudolf E. Anthelmintic flubendazole and its potential use in anticancer therapy. *Acta Medica (Hradec Kralove)*. 2017;60:5-11.
9. Meco D, Attinà G, Mastrangelo S, Navarra P, Ruggiero A. Emerging perspectives on the antiparasitic mebendazole as a repurposed drug for the treatment of brain cancers. *Int J Mol Sci*. 2023;24:1334.
10. Patil VM, Menon N, Chatterjee A, Tonse R, Choudhari A, Mahajan A, Puranik AD, Epari S, Jadhav M, Pathak S, Peelay Z, Walavalkar R, Muthuluri HK, Ravi Krishna M, Chandrasekharan A, Pande N, Gupta T, Banavali S, Jalali R. Mebendazole plus lomustine or temozolomide in patients with recurrent glioblastoma: a randomised open-label phase II trial. *EClinicalMedicine*. 2022;49:101449.
11. Patil VM, Bhelekar A, Menon N, Bhattacharjee A, Simha V, Abhinav R, Abhyankar A, Sridhar E, Mahajan A, Puranik AD, Purandare N, Janu A, Ahuja A, Krishnatry R, Gupta T, Jalali R. Reverse swing-M, phase 1 study of repurposing mebendazole in recurrent high-grade glioma. *Cancer Med*. 2020;9:4676-4685.
12. Mansoori S, Fryknäs M, Alvfors C, Loskog A, Larsson R, Nygren P. A phase 2a clinical study on the safety and efficacy of individualized dosed mebendazole in patients with advanced gastrointestinal cancer. *Sci Rep*. 2021;11:8981.
13. Larsen AR, Bai RY, Chung JH, Borodovsky A, Rudin CM, Riggins GJ, Bunz F. Repurposing the antihelmintic mebendazole as a hedgehog inhibitor. *Mol Cancer Ther*. 2015;14:3-13.
14. Zhang L, Bochkur Dratver M, Yazal T, Dong K, Nguyen A, Yu G, Dao A, Bochkur Dratver M, Duhachek-Muggy S, Bhat K, Alli C, Pajonk F, Vlashi E. Mebendazole potentiates radiation therapy in triple-negative breast cancer. *Int J Radiat Oncol Biol Phys*. 2019;103:195-207.
15. Wang X, Lou K, Song X, Ma H, Zhou X, Xu H, Wang W. Mebendazole is a potent inhibitor to chemoresistant T cell acute lymphoblastic leukemia cells. *Toxicol Appl Pharmacol*. 2020;396:115001.
16. Younis NS, Ghanim AMH, Saber S. Mebendazole augments sensitivity to sorafenib by targeting MAPK and BCL-2 signalling in n-nitrosodiethylamine-induced murine hepatocellular carcinoma. *Sci Rep*. 2019;9:19095. Erratum in: *Sci Rep*. 2022;12:13607.
17. Simbulan-Rosenthal CM, Dakshanamurthy S, Gaur A, Chen YS, Fang HB, Abdussamad M, Zhou H, Zapas J, Calvert V, Petricoin EF, Atkins MB, Byers SW, Rosenthal DS. The repurposed anthelmintic mebendazole in combination with trametinib suppresses refractory NRASQ61K melanoma. *Oncotarget*. 2017;8:12576-12595.
18. He L, Shi L, Du Z, Huang H, Gong R, Ma L, Chen L, Gao S, Lyu J, Gu H. Mebendazole exhibits potent anti-leukemia activity on acute myeloid leukemia. *Exp Cell Res*. 2018;369:61-68.
19. Walf-Vorderwülbecke V, Pearce K, Brooks T, Hubank M, van den Heuvel-Eibrink MM, Zwaan CM, Adams S, Edwards D, Bartram J, Samarasinghe S, Ancliff P, Khwaja A, Goulden N, Williams G, de Boer J, Williams O. Targeting acute myeloid leukemia by drug-induced c-MYB degradation. *Leukemia*. 2018;32:882-889.
20. Daniel JP, Mesquita FP, Da Silva EL, de Souza PFN, Lima LB, de Oliveira LLB, de Moraes MEA, Moreira-Nunes CFA, Burbano RMR, Zanatta G, Montenegro RC. Anticancer potential of mebendazole against chronic myeloid leukemia: *in silico* and *in vitro* studies revealed new insights about the mechanism of action. *Front Pharmacol*. 2022;13:952250.
21. Ariey-Bonnet J, Carrasco K, Le Grand M, Hoffer L, Betzi S, Feracci M, Tsvetkov P, Devred F, Collette Y, Morelli X, Ballester P, Pasquier E. In silico molecular target prediction unveils mebendazole as a potent MAPK14 inhibitor. *Mol Oncol*. 2020;14:3083-3099.
22. Nygren P, Fryknäs M, Agerup B, Larsson R. Repositioning of the anthelmintic drug mebendazole for the treatment for colon cancer. *J Cancer Res Clin Oncol*. 2013;139:2133-2140.
23. Blom K, Rubin J, Berglund M, Jarvius M, Lenhammar L, Parrow V, Andersson C, Loskog A, Fryknäs M, Nygren P, Larsson R. Mebendazole-induced M1 polarisation of THP-1 macrophages may involve DYRK1B inhibition. *BMC Res Notes*. 2019;12:234.
24. Zhu HL, Liu T, Meng WT, Jia YQ. [Establishment of an imatinib resistance cell line K562R and its resistant principia]. *Sichuan Da Xue*

Xue Bao Yi Xue Ban. 2007;38:22-26. Chinese.
25. Choi HS, Ko YS, Jin H, Kang KM, Ha IB, Jeong H, Song HN, Kim HJ, Jeong BK. Anticancer effect of benzimidazole derivatives, especially mebendazole, on triple-negative breast cancer (TNBC) and radiotherapy-resistant TNBC in vivo and in vitro. *Molecules*. 2021;26:5118.
26. Jafari R, Almqvist H, Axelsson H, Ignatushchenko M, Lundbäck T, Nordlund P, Martinez Molina D. The cellular thermal shift assay for evaluating drug target interactions in cells. *Nat Protoc*. 2014;9:2100-2122.
27. Fortin S, Lacroix J, Côté MF, Moreau E, Petitclerc E, C-Gaudreault R. Quick and simple detection technique to assess the binding of antimicrotubule agents to the colchicine-binding site. *Biol Proced Online*. 2010;12:113-117.
28. Berman HM, Battistuz T, Bhat TN, Bluhm WF, Bourne PE, Burkhardt K, Feng Z, Gilliland GL, Iype L, Jain S, Fagan P, Marvin J, Padilla D, Ravichandran V, Schneider B, Thanki N, Weissig H, Westbrook JD, Zardecki C. The Protein Data Bank. *Acta Crystallogr D Biol Crystallogr*. 2002;58:899-907.
29. Adasme MF, Linnemann KL, Bolz SN, Kaiser F, Salentin S, Haupt VJ, Schroeder M. PLIP 2021: expanding the scope of the protein-ligand interaction profiler to DNA and RNA. *Nucleic Acids Res*. 2021;49:W530-W534.
30. Zubair MS, Anam S, Khumaidi A, Susanto Y, Hidayat M, Ridhay A. Molecular docking approach to identify potential anticancer compounds from Begonia (*Begonia sp*). *AIP Conf Proc*. 2016;1755:080005.
31. Vitale I, Galluzzi L, Castedo M, Kroemer G. Mitotic catastrophe: a mechanism for avoiding genomic instability. *Nat Rev Mol Cell Biol*. 2011;12:385-392.
32. Sazonova EV, Petrichuk SV, Kopeina GS, Zhivotovsky B. A link between mitotic defects and mitotic catastrophe: detection and cell fate. *Biol Direct*. 2021;16:25.
33. Chen XH, Xu YJ, Wang XG, Lin P, Cao BY, Zeng YY, Wang Q, Zhang ZB, Mao XL, Zhang T. Mebendazole elicits potent antimyeloma activity by inhibiting the USP5/c-Maf axis. *Acta Pharmacol Sin*. 2019;40:1568-1577.
34. Freisleben F, Modemann F, Muschhammer J, Stamm H, Brauneck F, Krispien A, Bokemeyer C, Kirschner KN, Wellbrock J, Fiedler W. Mebendazole mediates proteasomal degradation of GLI transcription factors in acute myeloid leukemia. *Int J Mol Sci*. 2021;22:10670.
35. Ahearn I, Zhou M, Philips MR. Posttranslational modifications of RAS proteins. *Cold Spring Harb Perspect Med*. 2018;8:a031484.
36. Kolch W, Berta D, Rosta E. Dynamic regulation of RAS and RAS signaling. *Biochem J*. 2023;480:1-23.
37. Hentschel J, Rubio I, Eberhart M, Hipler C, Schiefner J, Schubert K, Loncarevic IF, Wittig U, Baniahmad A, von Eggeling F. BCR-ABL- and Ras-independent activation of Raf as a novel mechanism of Imatinib resistance in CML. *Int J Oncol*. 2011;39:585-591.
38. Ma L, Shan Y, Bai R, Xue L, Eide CA, Ou J, Zhu LJ, Hutchinson L, Cerny J, Khoury HJ, Sheng Z, Druker BJ, Li S, Green MR. A therapeutically targetable mechanism of BCR-ABL-independent imatinib resistance in chronic myeloid leukemia. *Sci Transl Med*. 2014;6:252ra121.
39. De Witt M, Gamble A, Hanson D, Markowitz D, Powell C, Al Dimassi S, Atlas M, Boockvar J, Ruggieri R, Symons M. Repurposing mebendazole as a replacement for vincristine for the treatment of brain tumors. *Mol Med*. 2017;23:50-56.
40. Elayapillai S, Ramraj S, Benbrook DM, Bieniasz M, Wang L, Pathuri G, Isingizwe ZR, Kennedy AL, Zhao YD, Lightfoot S, Hunsucker LA, Gunderson CC. Potential and mechanism of mebendazole for treatment and maintenance of ovarian cancer. *Gynecol Oncol*. 2021;160:302-311.
41. Bai Y, Hou Y, Wang Q, Lu C, Ma X, Wang Z, Xu H. Analysis of the binding modes and resistance mechanism of four methyl benzimidazole carbamates inhibitors fungicides with *Monilinia fructicola* β2-tubulin protein. *J Mol Struct*. 2023;1291:136057.
42. Kipper FC, Silva AO, Marc AL, Confortin G, Junqueira AV, Neto EP, Lenz G. Vinblastine and antihelmintic mebendazole potentiate temozolomide in resistant gliomas. *Invest New Drugs*. 2018;36:323-331.
43. Skibinski CG, Williamson T, Riggins GJ. Mebendazole and radiation in combination increase survival through anticancer mechanisms in an intracranial rodent model of malignant meningioma. *J Neurooncol*. 2018;140:529-538.
44. Markowitz D, Ha G, Ruggieri R, Symons M. Microtubule-targeting agents can sensitize cancer cells to ionizing radiation by an interphase-based mechanism. *Onco Targets Ther*. 2017;10:5633-5642.